Point Cloud Neighborhood Estimation Method Using Deep Neuro-Evolution

Ahmed Abouelazm, Igor Vozniak, Nils Lipp, Pavel Astreika and Christian Mueller
Deutsches Forschungszentrum für Künstliche Intelligenz (DFKI), Saarbruecken, Germany

Keywords: Point Clouds, 3D Deep Learning, Neighborhood Estimation, Deep Neuro-Evolution.

Abstract: Due to the recent advancements in computing hardware, deep learning, and 3D sensors, point clouds have become an essential 3D data structure, and their processing and analysis have received considerable attention. Given the unstructured and irregular nature of point clouds, encoding local geometries is a significant barrier in point cloud analysis. The aforementioned challenge is known as neighborhood estimation, and it is commonly addressed by fitting a plane to points within a local neighborhood defined by estimated parameters. The estimated neighborhood parameters for each point should adapt to the point cloud's irregularities and different local geometries' sizes and shapes. Different objective functions have been derived in the literature for optimal parameters selection with no efficient approach for these objective functions' optimization as of now. In this work, we propose a novel neighborhood estimation pipeline for such optimization which is objective function and neighborhood type invariant, utilizing a modified version of deep Neuro-Evolution algorithm and Farthest Point Sampling as an intelligent sampling approach. Results demonstrate the ability of the proposed pipeline for state-of-the-art objective functions optimization and enhancement of neighborhood properties estimation such as the normal vector.

1 INTRODUCTION

RGB images have long been the focus of image processing and computer vision research. Furthermore, the fast development of deep learning has aided the rise of 2D images as a dominant data structure (Chai et al., 2021). However, we live in a three-dimensional world, and the capacity of two-dimensional images to fully depict three-dimensional objects in the world is limited. This is due to the fact that RGB images do not capture depth information and instead project data on a single depth 2D plane. Furthermore, RGB images are sensitive to illumination and lack contrast. Due to the importance of depth information in understanding the geometry of a scene, algorithmic techniques for depth estimation from single and stereo images have been investigated in the literature (Ming et al., 2021; Lazaros et al., 2008). Despite the success of these techniques, 3D sensors that can directly capture depth without estimation are required. Thus, several 3D data formats have been proposed in recent years, such as point clouds and RGB-D images. Due to the rapid development of 3D acquisition devices such as LiDAR and RGB-D sensors, as well as the decrease in their cost, 3D data structures have been expanded to a variety of applications nowadays such as robotics and autonomous driving (Royo and Ballesta-Garcia, 2019). One of the most prevalent 3D data structures

Figure 1: Challenge of neighborhood estimation on an irregular point cloud (Bello et al., 2020), as the point cloud has sparse and dense regions, which requires adapting neighborhood parameters.

is Point Cloud Data (PCD), which is a representation generated by LiDAR sensors. PCD is a 3D format that depicts a scanned object as a set of discrete points scattered in a Euclidean space. Each point representation can be augmented by color, normal vector at the point of interest, and other feature descriptors. Despite becoming increasingly popular in the research community, PCDs still face the following main disadvantages which must be considered during analysis and processing. PCD is an unordered set of points that lacks any underlying structure or regular grid. Besides, it is an irregular data type with some regions having high density, large number of points per unit

Abouelazm, A., Vozniak, I., Lipp, N., Astreika, P. and Mueller, C.
Point Cloud Neighborhood Estimation Method Using Deep Neuro-Evolution.
DOI: 10.5220/0011627300003417
In *Proceedings of the 18th International Joint Conference on Computer Vision, Imaging and Computer Graphics Theory and Applications (VISIGRAPP 2023) - Volume 4: VISAPP*, pages 582-593
ISBN: 978-989-758-634-7; ISSN: 2184-4321
Copyright © 2023 by SCITEPRESS – Science and Technology Publications, Lda. Under CC license (CC BY-NC-ND 4.0)

volume, whereas others are sparse, with just a few points as depicted on figure 1.

The challenges as mentioned earlier require permutation invariant density aware methods for encoding local geometries and local correlations between points in a PCD. Local geometries are commonly encoded by extracting features from a plane fitted to a neighborhood, where the points included in the neighborhood are determined by a set of parameters, for each point in the PCD. The estimation of these parameters is known as neighborhood estimation (Weinmann et al., 2015; Demantké et al., 2011), and it is a critical step for the majority of machine learning techniques used in PCD processing. Since the attributes initially retrieved using neighborhood estimation can be used for more complex tasks such as keypoints detection and feature descriptors (Cirujeda et al., 2014; Huang and You, 2012; Siritanawan et al., 2017; Zhong, 2009). Furthermore, neighborhood estimation is not only essential for machine learning techniques but has also been integrated into deep learning modules (Liu et al., 2019; Suo et al., 2020; Zhao et al., 2022; Yang et al., 2018).

Due to the obvious irregular nature of PCDs, as illustrated on figure 1, fitting a neighborhood with the same parameters throughout the PCD is inappropriate as these parameters should vary between dense and sparse regions and take into account the dimensionality and size of local geometries present in the PCD. In the literature, several neighborhood types and two objective functions have been proposed for optimal neighborhood estimation (Weinmann et al., 2015; Demantké et al., 2011). However, to the best of our knowledge, no effective pipeline exists to optimize these suggested objective functions, except for a grid-based search with fixed resolution presented in (Demantké et al., 2011; Weinmann et al., 2015). The proposed grid search requires exhaustive iteration over a discrete set of neighborhood parameters fixed for all points, and doesn't have the ability to generalize to similar points.

*The contribution of this work is the design and validation of a novel and computationally efficient (requires fewer training parameters; no back-propagation step is involved, thus, less used memory) pipeline for explicit and optimal neighborhood estimation using a learning module in an **unsupervised manner***. The learning module learns optimal parameter selection from a small subset of points and generalizes the learned selection across the remaining points in the PCD, thus enhancing computation and memory efficiency while finding an accurate solution. An effective subset of points for learning is sampled using Farthest Point Sampling (FPS) (Eldar et al., 1994) as it has the ability to sample points that provide sufficient information about the point cloud structure. The novelty of this work is twofold: a) we propose to use a modified version of Deep Neuro-Evolution (Salimans et al., 2017) as a learning module such that parameter selection can be learned over the sampled points, and the learned selection can generalize for unseen points that have similar points distribution in their vicinity. We employ Deep Neuro-Evolution as it is able to handle non-differentiable objectives such neighborhood estimation with minimal memory and computation loads. b) Additionally, we propose, a novel heuristic function to guide the learning module search, rejecting trivial solutions of empty neighborhoods.

2 RELATED WORK

The standard approach for encoding local geometries in PCDs is fitting a plane to a neighborhood centered at the point of interest. The approximate plane eigenvalues and eigenvectors are used to estimate key properties of the interest point such as normal vector, principle curvature and surface variation (Weinmann et al., 2014). As a result, the neighborhood estimation procedure is a critical component of a number of PCD applications such as keypoints detection and features description and have been integrated into deep learning modules. Figure (2) illustrates neighborhood estimation and its various applications. In this section, we provide an overview of related work, relevant for the objectives of this work.

2.1 Neighborhood Types

There are two types of neighborhoods commonly used in PCDs analysis: spatial-based and similarity-based neighborhoods, as categorized in (Weinmann et al., 2014). Spatial neighborhoods assign points to a neighborhood v_p^r centered around the center point p, if the points are located in the interior surface of a parameterized geometry representing the neighborhood. The spherical neighborhood is the most commonly used 3D spatial neighborhood. Spherical neighborhood fits a sphere parameterized by radius r to a center point p, and a point q belongs to the neighborhood of p when the Euclidean distance between them is smaller than the radius, as shown in equation (1). Cylindrical neighborhood is another variant of spatial based neighborhoods, which centers an infinitely long vertically oriented cylinder with a radius r at a center point p, as discussed in equation (2) with the height as the z direction. This neighborhood can be conceived

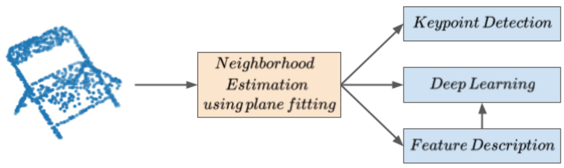

Figure 2: Point cloud neighborhood estimation and its various applicability cases.

as the projection of points onto a plane with a constant height and the assignment of points to the neighborhood that are located within a circle of radius r.

$$r \in \mathbb{R},\ v_p^r = \{q \mid d(q,p) \leq r\} \tag{1}$$

$$r \in \mathbb{R},\ v_p^r = \left\{q \mid \left[(p_x - q_x)^2 + (p_y - q_y)^2\right]^{\frac{1}{2}} \leq r\right\} \tag{2}$$

K-nearest neighborhoods is the most commonly utilized similarity neighborhood. The k-nearest neighborhood computes a similarity metric over all points in the PCD. The top-k similar points are included in the final neighborhood. The Radial Basis Function (RBF) kernel with a unit variance of the Euclidean distance between the center point p and the surrounding points q is a regularly used similarity metric.

2.2 Plane Fitting

Following the selection of a neighborhood type and parameters, relevant information is extracted from the covariance matrix computed over the neighborhood's points. As described in equation (3), the covariance matrix is a symmetric positive semi-definite matrix computed using statistics over points within a neighborhood v_p^r centered at point p and parameterized by r. The eigenvalues and eigenvectors of the covariance matrix, recovered via eigenvalue decomposition as seen in equation (4), are used to approximate the fitted plane.

$$Cov(v_p^r) = \frac{1}{|v_p^r| - 1} \sum_{q \in v_p^r} (q-\mu)^T \times (q-\mu) \tag{3}$$

$$\lambda \times Cov(v_p^r) = \lambda \times v \tag{4}$$

2.3 Keypoints Detection

The majority of keypoints detection algorithms are dependent on neighborhood estimation as an initial processing step. Keypoints detection extracts points with unique features within a local vicinity in a PCD. ISS (Zhong, 2009) defines keypoints as points with high 3D variation (smallest eigenvalue of the approximate plane) within a local vicinity. To eliminate any ambiguity in keypoints, ISS employs two pruning techniques: points with equal eigenvalues omission and resolution control. SURE (Fiolka et al., 2012) investigates the ratio between the approximated plane's maximum and minimum eigenvalues. Keypoints are detected by applying a threshold operator on the investigated ratio.

MSV (Siritanawan et al., 2017) and MoPC (Huang and You, 2012) apply multi-scale analysis by fitting neighborhoods of different scales to a point of interest. The scales range between minimum and maximum scales $[s_{min}, s_{max}]$ and are increased with a discrete step size. MSV keypoints are points whose surface variation (smallest normalized eigenvalue of the approximate plane) averaged over all scales is higher than a certain threshold. MoPC, on the other hand, selects keypoints based on principle curvature (largest eigenvalue of the approximate plane). A point at a given scale s_n is considered a keypoint if it has the largest principle curvature, when compared to both, the same point at the previous scale s_{n-1} and the subsequent scale s_{n+1}, and all its neighbors that lie within a third of the scale $\frac{1}{3}s_n$ of the point.

2.4 Features Description

The detection of keypoints is followed by a description of their features in the encoding pipeline. The aim of features description is to provide an extended features vector for a more meaningful embedding of PCD. (Vandapel et al., 2004) proposed a linear combination of the eigenvalues of the estimated plane of the keypoint, yielding an eigenvalue-based descriptor which is resilient against rigid transformations. RSD (Marton et al., 2010) models a radial relationship between a keypoint and its neighbors by the distance between them and the angle between their normals. The final descriptor is minimum and maximum radius attained within a neighborhood. (Triebel et al., 2006) utilized a 1D histogram of cosine angles between a keypoint and its neighborhoods normal vectors as a descriptor. Thrift (Flint et al., 2007) is another approach that uses 1D histograms of cosine angles, with the angle defined between normal vectors computed on two different scales for the same keypoint neighbor.

Spin Image (Johnson and Hebert, 1998) calculates two geometric features (α, β) between a keypoint p and its neighbor q by aid of the neighbor's normal vector n_q. A 2D histogram over α, β of the keypoint neighborhood is the proposed descriptor. The approach of PFH (Rusu et al., 2008b; Rusu et al., 2008a) is similar to that of Spin Image. Given a keypoint p and a pair of its neighbors, q_s and q_t, a darboux frame is constructed based on the distance between the pair and the normal vector of q_s. Four geometric properties are derived using the darboux frame, and the final PFH descriptor is a 4D histogram that incorporates these properties.

2.5 Deep Learning

The neighborhood estimation task has been used in a number of deep learning modules. PointNet (Qi et al., 2017a) is a pioneer work in deep learning on the raw data of PCDs. Even though this network provided advancement in the field and sparked huge interest in learning from raw PCD, it lacked the ability to capture the correlation between neighboring points and complex local geometries. Thus, (Qi et al., 2017b) proposed PointNet++ to overcome this drawback by hierarchical learning contextual information over a PCD. PointNet++ samples a subset of points from a PCD and groups points in a fixed radius, fixed neighborhood parameter, around the sampled points using a sampling and grouping layer. The grouped points in the local neighborhood are processed using PointNet to extract useful information. DGCNN (Wang et al., 2019) constructs a *k*-nearest neighbors graph with fixed K and uses an edge convolution layer to learn from its constructed input. FoldingNet (Yang et al., 2018) is a PCD auto-encoder architecture used for reconstruction task. This architecture appends the local covariance matrix of each point, calculated using a *knn*-neighborhood with K=16 as described in equation (3), to the input feature vector. Both LPD-Net (Liu et al., 2019) and its successor LPD-AE (Suo et al., 2020) merge ten features that were retrieved from the fitted neighborhood with the input points coordinates. The empirical results in the aforementioned papers and their analysis showed that selecting the optimal neighborhood size rather than a fixed one improved network performance and recall ability. However, a grid search with fixed resolution over neighborhood parameters was used, which has the drawback of requiring a large amount of memory and computing load. (Zhao et al., 2022) dedicated a separate branch to extracting information from features computed over a *knn*-neighborhoods with constant size for all points. The retrieved features are calculated using local frames constructed between a center point p and its neighbor q, and are then fused with extracted features from spatial information to form a single descriptor. The addition of such features increased the network's robustness against rigid input transformations.

2.6 Neighborhood Estimation Objective Functions

(Demantké et al., 2011) identifies two major issues with selecting neighborhood parameters: it cannot be chosen heuristically, and it cannot be constant over the whole PCD. Instead, it should be directed by data and tailored to varying densities and sizes of PCD local geometries.

(Demantké et al., 2011) introduces two objective functions for selecting neighborhood parameters. The goal of such functions is to automate the selection of the optimal neighborhood parameters for each point in a PCD. Both objective functions are based on a point's dimensionality features, as described in (Toshev et al., 2010). These features are calculated based on eigenvalues ordered in descending order as depicted in equation (5), where a_{1D}, a_{2D}, and a_{3D} represent the degree of linearity, planarity, and scattering exhibited by a point p when a neighborhood $\boldsymbol{v}$ parameterized by r is centered around p. The dimensionality label of a point p is the degree with the highest value as provided in equation (6), where $\lambda_1 \geq \lambda_2 \geq \lambda_3$ represent the eigenvalues of the approximate plane in descending order.

$$a_{1D} = \frac{\lambda_1 - \lambda_2}{\lambda_1},\ a_{2D} = \frac{\lambda_2 - \lambda_3}{\lambda_1},\ a_{3D} = \frac{\lambda_3}{\lambda_1} \tag{5}$$

$$d^*(v_p^r) = \underset{d\in[1,3]}{\arg\max}\, a_{dD} \tag{6}$$

The first objective function defines the optimal parameters as the parameters that minimize the Shannon entropy of the dimensionality features within a neighborhood, as described in equation (7, 8). The intuition behind such an objective function is finding parameters which favors a single dimensionality within the neighborhood.

$$E(v_p^r) = -a_{1D}\ln(a_{1D}) - a_{2D}\ln(a_{2D}) - a_{3D}\ln(a_{3D}) \tag{7}$$

$$r_{optimal} = \underset{r}{\arg\min}\, E(v_p^r) \tag{8}$$

The other objective function supports picking a neighborhood with the majority of points labeled with the same dimensionality (homogeneous), as shown in equations (9, 10).

$$S(v_p^r) = \frac{1}{n}\sum_{q\in v_p^r} 1_{\{d^*(v_p^r)=d^*(v_q^r)\}} \tag{9}$$

$$r_{optimal} = \underset{r}{\arg\max}\, S(v_p^r) \tag{10}$$

In the aforementioned work, both objective functions were optimized using grid search with a predefined resolution bounded between (r_{min}, r_{max}). When compared to homogeneity-based criteria, the reported results show that dimensionality-based entropy criteria are more desirable since they can have a unique solution per point and do not saturate.

An alternative entropy based objective function is introduced in (Weinmann et al., 2015). Unlike dimensionality-based functions, this function seeks to reduce the Shannon entropy of the normalized eigenvalues, as proposed in equations (11, 12). The idea behind such a function is to decrease noise and uncertainty in the selected neighborhood eigenvalues.

$$\varepsilon_i = \frac{\lambda_i}{\lambda_1 + \lambda_2 + \lambda_3} \tag{11}$$

$$E(v_p^r) = -\varepsilon_1 \ln(\varepsilon_1) - \varepsilon_2 \ln(\varepsilon_2) - \varepsilon_3 \ln(\varepsilon_3) \tag{12}$$

3 METHODOLOGY

As discussed in Section 2 and illustrated in figure (2), explicit neighborhood estimation is an essential preprocessing step for efficient PCD analysis. In this work, we propose a pipeline for explicit and optimal neighborhood estimation. The pipeline doesn't require supervision or access to ground truth information such as normal vectors or curvatures. It is worth mentioning that the estimated neighborhoods are task-agnostic, with desirable properties due to the choice of the objective function. Additionally, the neighborhood is designed with low memory and computation footprint to accelerate the task significantly.

A pipeline for neighborhood estimation that is both memory and computationally efficient is lacking in the literature, since only grid search with a fixed resolution was used to minimize objective functions addressed in Section 2.6. The two objective functions depicted in equations (7, 12) are used for automated neighborhood estimation in this work. The third objective function presented in equation (9) is disregarded as it has a combinatorial nature, and empirical results reported in (Demantké et al., 2011) demonstrate that it performs poorly when compared to the other two. In this work, we focus on increasing the task efficiency by learning the optimal neighborhood parameter choice over a small subset of points from a PCD driven by the aforementioned objective functions and then generalizing this learning across the remaining points.

This work adopts and modifies Deep Neuro-Evolution (Salimans et al., 2017) as the building block of the proposed pipeline. To the best of our knowledge, this work is the first in modifying Deep Neuro-Evolution as a parameter estimation module. Deep Neuro-Evolution (Such et al., 2017) is a non-gradient-based alternative to deep reinforcement learning and is described as the successor to evolution strategies introduced in (Salimans et al., 2017). Evolution Strategies (ES) is a gradient-based deep evolution technique that produces results comparable to Q-learning and policy gradient approaches (Salimans et al., 2017). ES evaluates a network at a number of mutations generated by random noise. A gradient approximated by a modified finite-difference operation is used to update the network parameters. The success of ES sparked interest in developing an entirely gradient-free technique based on evolutionary algorithms that can scale effectively as a deep reinforcement learning alternative, leading to the formulation of Deep Neuro-Evolution. In comparison to deep reinforcement learning and ES, Deep Neuro-Evolution has a sizable advantage in the neighborhood estimation problem and requires far less memory compared to reinforcement learning because it does not require state representation or buffer memory. Additionally, since Deep Neuro-Evolution does not require back-propagation, it requires less computational effort than approaches as in (Such et al., 2017). Furthermore, it can also be used in a distributed manner over multiple threads.

Preliminaries. Deep Neuro-Evolution is a variant of the standard genetic algorithm, in which each individual (genotype) is a neural network. A mutation function ψ, network initialization method ϕ, and fitness function F are all required by the algorithm in addition to the number of individuals in each generation, the number of generations, and the number of top T performing individuals to keep for next generations. The mutation function ψ modifies the network's weights to generate a new individual, while the network initialization ϕ provides a deterministic method for creating the initial network's weights. Finally, the fitness function is utilized to assess each individual's performance.

Our proposed Deep Neuro-Evolution uses a shallow version of PointNet (Qi et al., 2017a) as an individual, which uses blocks of Multi-Layer Perceptron (MLP) and Relu Nonlinearity to process each point in the input individually. In this work, the shallow network has two PointNet blocks, thus having very few learnable parameters, decreasing the computation load. The second block's output is collapsed by max pooling, as it is a permutation invariant function due to its symmetric nature, into a global description. A linear layer is added after the global description vector to obtain the network's final output. The network input is the PCD centered around the point of interest p for which the neighborhood is estimated. Moreover, the network computation can be enhanced by

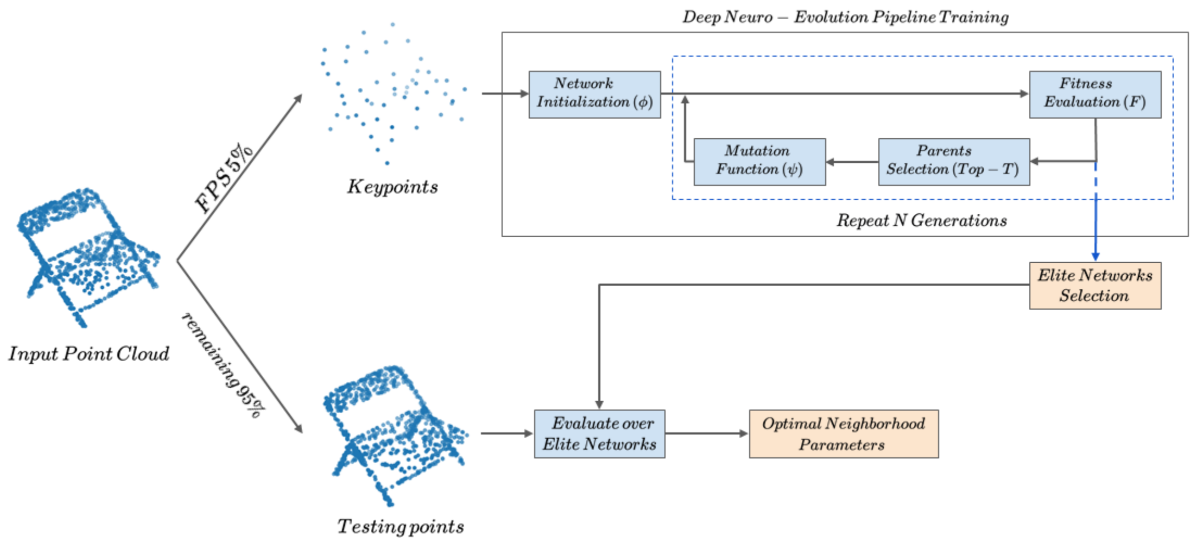

Figure 3: Pipeline overview. A subset of points is sampled using FPS, which are used to train the proposed pipeline. The proposed pipeline searches for the Elite Networks for the neighborhood estimation task. The Elite Networks are subsequently used to estimate parameters of the remaining points.

only taking a sufficient subset of the PCD around the point of interest. The network output is the neighborhood parameterization and is subjected to a *tanh* non-linearity to constrain it to the range [-1, 1], after which it is remapped to fulfil the chosen parameter limits.

Deep Neuro-Evolution searches for the fittest individual (Elite) among those created over G generations. The fitness of each individual in estimating a neighborhood for a center point p is evaluated using our novel fitness function proposed in equation (13). The fitness function's first term is in charge of promoting neighborhood parameter selection that minimizes neighborhood entropy and represents the difference between the maximum Shannon entropy of a neighborhood defined over three random variables (x, y, z), which is equal to $\ln(3)$, and the neighborhood entropy obtained with network estimated parameters r_i. As a consequence, the fittest parameter choice is the one with the lowest entropy, as required by equation (8). Furthermore, this term is independent of the entropy function employed, and it can be calculated using either the eigen entropy or the dimensionality entropy stated in equations (7, 12). The second term of equation (13) is responsible for penalizing neighborhoods with less than two points in the neighborhood, since this is a trivial solution and doesn't provide any tractable information about the center point p.

$$F(\theta_i) = \left[\,\ln(3) - E(v_p^{r_i})\,\right] + \ln(3) \times \mathbf{1}_{|v_p^{r_i}|>2} \tag{13}$$

In the initial generation, $N-1$ individuals are created with randomly initialized weights using the Xavier uniform initialization (Glorot and Bengio, 2010). The benefit of this initialization is that the network is not biased towards any single region in the search space, but instead has a uniform distribution of output over the whole search space.

For subsequent generations, one of the top T-performing parents is uniformly sampled at random. The sampled parent weights are mutated by applying an additive Gaussian noise regulated by a hyperparameter σ as seen in equation (14), to generate a new individual which explores a slightly different region in the search space. The hyperparameter σ controls how dispersed the new individual is from its parent in the search space. A high sigma value causes significant jumps in the search process, whereas a low sigma causes the search to be localized and limited to a certain region of the search space. As a result, the initial value of σ is obtained empirically during experiments, and σ decays at a linear rate every generation, allowing the search to be more localized in the fittest areas of the search space as the number of generations increases. This concept is parallel to the exploration-exploitation trade-off in reinforcement learning (Salimans et al., 2017).

$$\begin{gathered} \varepsilon \sim \mathcal{N}(0, I) \\ \theta^n = \psi(\theta^{n-1}, \varepsilon) = \theta^{n-1} + \sigma \times \varepsilon \end{gathered} \tag{14}$$

Each mutated individual performance is evaluated using fitness function F. Consequently, the generated individuals are ordered in a descending manner based on their fitness score. The set of elite candidates is established through truncation selection, which involves picking the top T-performing parents. The elite individual, the best performing one globally during the search process thus far, is updated by comparison to the maximum argument over the candidate set and appended to the candidate set if not already a member. The elite individual (network) with the fittest neighborhood parameters is returned as the algorithm output once all generations have been generated. This elite individual can be utilized in estimating neighborhood parameters for other points that exhibit similar geometric and spatial properties.

Even though the adapted Deep Neuro-evolution approach has low memory and processing, it is inefficient for estimating neighborhood parameters per point, especially on large scale PCDs with millions of points. It is more efficient to learn the parameter search using Deep Neuro-evolution over a small sample of points, 5% of the points in the PCD, and then applying the learned search over the remaining 95% unseen points in the PCD. The overall pipeline pseudocode is illustrated in algorithm 1. It should be highlighted that pipeline efficiency in both the Deep Neuro-evolution (lines 2–5) and the elite networks' evaluation (lines 6–14) stages are further improved by utilizing a relevant subset of points as the network input instead of the whole PCD e.g. the points included within the neighborhood defined by the maximum parameter. Additionally, a visual clarification of the proposed pipeline can be seen in figure (3).

Different sampling techniques have been proposed in the literature to extract keypoints from a PCD as discussed in Section 2.3. However, since most of these approaches rely on neighborhood estimation, using them in the proposed pipeline is contradictory. Whereas, random sampling and FPS were described as effective keypoints sampling alternatives for PCD in (Varga et al., 2021; Qi et al., 2017b) respectively. Random sampling draws a subset of points from a PCD uniformly at random. FPS, on the other hand, is an iterative sampling technique that starts with a random point as a seed and samples the PCD's farthest point from the previously sampled seed as the new seed in an iterative manner. In this work, FPS is preferable since it captures the PCD structure and summarizes its details in a few points, whereas random sampling loses shape details and rough structure, and can easily hinder the pipeline performance, as shown by the example on figure (4c).

Classical multi-scale shape analysis (Demantké et al., 2011) proposes multiple analysis scales fixed for all points, which are not tailored by the data. Our pipeline is more effective than multi-scale analysis since it requires less computational power and directly extracts a single optimal value for each parameter, which can then be used for the precise estimation of a center point characteristics like normal vectors and curvatures and employed in clustering frameworks like the region growing algorithm (Rabbani et al., 2006). Furthermore, our pipeline is easily extensible as an enhanced multi-scale analysis approach by altering the pipeline's output to be the $top-k$ elite individuals for each point in the keypoints, hence strengthening the multi-scale analysis by selecting informative scales based on geometric and spatial properties of points rather than a pre-defined set identical for all points.

It is essential to emphasize, that the proposed pipeline is an *unsupervised* approach guided by a novel objective function for hard assignment of local neighborhoods. There are other approaches that focus on soft assignment of neighborhoods, such as (Ben-Shabat et al., 2019; Zhou et al., 2021a; Ben-Shabat and Gould, 2020; Zhu et al., 2021; Zhou et al., 2021b). The soft assignment is established for a center point by learning weights over neighboring points on a rather big neighborhood size fixed for all center points. However, the aforementioned approaches are trained in a *supervised manner* to minimize normal estimation loss given its ground truth and uti-

Algorithm 1: The proposed pipeline Pseudocode.

Require: mutation function ψ, population size N, number of selected individuals T, number of generations G, network initialization routine ϕ, fitness function F, point cloud P
1: sample 5% of the total points in P as keypoints Q using FPS as in line with (Qi et al., 2017b)
2: **for** each keypoint q in Q **do**
3: elite ← Deep Neuro-Evolution(ψ, N, T, G, ϕ, F, P centered around q) as in line with (Such et al., 2017)
4: Elite networks ← Elite networks ∪ elite
5: **end for**
6: **for** each remaining point p in $P \setminus Q$ **do**
7: **for** each elite in Elite networks **do**
8: neighborhood parameters ← elite (P centered around p)
9: neighborhood fitness ← F (neighborhood parameters)
10: **if** best fitness < neighborhood fitness **then**
11: best fitness ← neighborhood fitness
12: optimal parameters ← neighborhood parameters
13: **end if**
14: **end for**
15: Per-point parameters ← Per-point parameters ∪ optimal parameters
16: **end for**
17: **return** Per-point parameters

SCITEPRESS SCIENCE AND TECHNOLOGY PUBLICATIONS

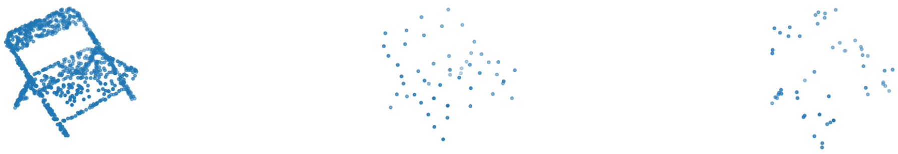

(a) Input point cloud. (b) Output point cloud using FPS. (c) Output point cloud using random sampling.

Figure 4: Output point clouds of a chair class from different sampling techniques. The output illustrates that FPS is favorable than random sampling as it has the ability to summaries a point cloud in few points while maintaining its structure.

lize a large patch of points around a center point without explicit extraction of neighborhood parameters. Whereas, our method explicitly extracts neighborhood parameters and is task-agonistic such that the neighborhood has desired properties that can be later fine-tuned for specific tasks such as the ones discussed in Section 2, which are out of the scope of this research. Moreover, in (Zhou et al., 2021b), one of the best-performing networks on supervised normal estimation, authors reported that utilization of a first-order jet fitting, equivalent to the plane fitting used in our work, and $top-k$ selection strategy enhances normal estimation results. The $top-k$ selection only uses information from the $top-k$ critical points for fitting, however, it is manually set and fixed for all points. In our paper, we provided a method for the dynamic setting of the k parameter of an unweighted fitting approach. Furthermore, our work can directly benefit pre-processing steps of other approaches such as (Yang et al., 2018; Suo et al., 2020; Liu et al., 2019), which the aforementioned approaches cannot contribute to. Finally, the proposed approach has considerably fewer learnable parameters than all other networks and can be used to estimate parameters for a single PCD without any pre-training. For future work, it is planned to integrate both jet fitting and weighted neighborhoods in our pipeline while keeping its unsupervised setting.

4 EVALUATION

4.1 Dataset

In this work, ModelNet-10 dataset is used for the evaluation purposes of the proposed neighborhood estimation pipeline. ModelNet-10 is a benchmark for 3D object classification and retrieval published by Princeton University in (Wu et al., 2015). The dataset contains, 4899 CAD-generated meshes stored in Object File Format (OFF), which are divided into 3991 meshes for training and 908 meshes for testing purposes. Moreover, it is well known in the research community since it is a well-structured dataset with

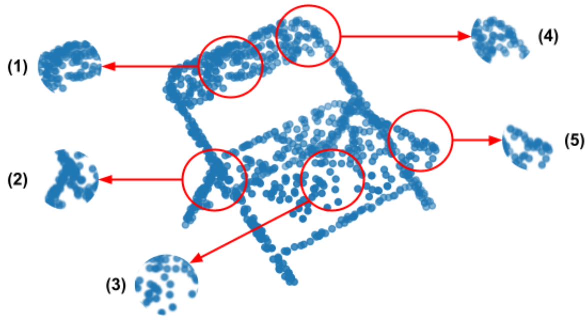

Figure 5: Different examples of points irregularity and complex features that require the adaptation of the neighborhood parameters.

pre-aligned clean shapes sampled from several categories. Currently, the dataset has ten classes: bathtub, bed, chair, desk, dresser, monitor, nightstand, sofa, table, and toilet. An output PCD is generated by randomly sampling points from the CAD-generated mesh's triangular faces, which enforces the existence of irregularities in the PCD. The sampled points are normalized and fitted into a bounding box between $[-1,1]$. Even though ModelNet 10 dataset is a clean and aligned dataset, it contains a variety of objects with complex geometries that necessitate the adaptation of the neighborhood parameters. Figure (5) illustrates an example of a PCD from class chair. Different regions with less dense points distribution and irregular nature are highlighted in figure (5: sub-figures 2 and 5). Additionally, these examples clarify that edges, corners and other fine details require adaptation of the neighborhood parameters to be captured correctly compared to points belonging to coarser features such as the seat or the back of the chair as depicted in figure (5: sub-figures 3, 1, 4 respectively).

4.2 Evaluation Metrics

A k-nearest neighborhood using RBF kernel of Euclidean distance as a similarity metric and constant size $K = 30$ is utilized as a baseline against which this work was evaluated, which is the standard approach for fitting a neighborhood to the ModelNet-10 dataset (Qi et al., 2017b; Wang et al., 2019). The primary evaluation metrics in this work are: **a) the minimization of eigen entropy** and **b) minimization of dimensionality entropy** objective functions formulated in equations (7, 12) respectively. These two objective functions are reviewed in the literature (Demantké et al., 2011; Weinmann et al., 2015), where achieving lower entropy implies the choice of more optimal parameters. The entropy minimization evaluations demonstrate the pipeline's efficiency of its optimization characteristics and ability to generalize for learning over only a small subset of points in the PCD.

Despite the fact that neighborhood estimation is explicitly correlated to the normal estimation task for a PCD, we, additionally, use our pipeline to investigate the impact of optimal neighborhood selection on such a task . In our work, the normal vector at a point in the PCD is approximated by the eigenvector of the smallest eigenvalue of the estimated neighborhood at the point. Besides, the unoriented angle similarity and the proportion of good points (PGP) as introduced in (Wang and Prisacariu, 2020) are used to assess the quality of the normal estimation. As seen in equation (16), the unoriented angle similarity measures the similarity between the estimated normal vector $\hat{n}$ and a ground truth normal vector n, which is the normal vector at the triangular face from which the point is sampled. The unoriented angle similarity calculates the similarity by first computing the angle β between $\hat{n}$ and n as in equation (15), and then normalizing the angle β by the maximum angular difference β_{max}, which in this case is set to 90°. The percentage of good points (PGP) is another evaluation metric for normal estimation tasks, where PGP_α denotes the percentage of points having a normal estimation error of less than α, as seen in equation (17). Crucially, we assess the proposed pipeline over normal estimation task only since it has the aforementioned metrics of evaluation, whereas keypoint detection and feature description have no quantitative evaluations and are instead evaluated qualitatively which is inconclusive. Furthermore, we compare our pipeline against the classical Principal Components Analysis (PCA), as discussed in (Demantké et al., 2011), since it computes normal vectors in an unsupervised manner and our pipeline serves as a pre-processing step for choosing meaningful parameters to be used by PCA.

$$\beta = arccos\left(\left| \frac{\hat{n} \cdot n}{\|\hat{n}\| \, \|n\|} \right| \right) \tag{15}$$

$$similarity(\beta) = 1 - \frac{\beta}{\beta_{max}} \tag{16}$$

$$PGP_\alpha = \frac{1}{N} \sum_{a \in P} \mathbf{1}_{\beta_a < \alpha} \tag{17}$$

4.3 Training Setting

The implementation of the proposed pipeline is realized in Python 3.9 and PyTorch 1.10.0 without utilizing GPUs or parallel threading. Even though a GPU-enabled implementation is available and a parallel threading version of the pipeline, in which different keypoints can be deployed on multiple threads, can be adapted in a straightforward manner for faster execution. The lightweight PointNet blocks have 16 output features each, where the network weights are initialized using Xavier uniform initialization and the biases are set to 0.01. The hyperparameter σ of the mutation function, as described in equation (14), is set to 0.3 and decay linearly with 0.05 at each generation. Given each keypoint, the modified deep Neuro-Evolution runs for 5 generations with a population size of 50 individuals and keeps the top 20 performing individuals at each generation to act as parents of the subsequent generation.

4.4 Results

Table 1 illustrates the eigen and dimensionality entropy produced by our pipeline in different neighborhood types, compared to the classical baseline. This table is dedicated to the results of the training and testing points. Training points are points sampled with FPS and passed in an unsupervised training manner to Deep Neuro-evolution. A total of 1028 points are sampled from each mesh, however, only 51 points are used for training. The findings indicate that independent of the neighborhood type, our proposed pipeline attains lower (better) entropy values compared to the baseline. The test points are the 95% remaining points that were not included in the pipeline training. Results show that the pipeline has a good generalization performance over the unseen points. These results support our hypothesis that when directed by the novel fitness function provided in equation (13), an intelligent sampling approach (FPS) and Deep Neuro-Evolution as a learning algorithm an effective and novel pipeline for neighborhood estimation is proposed.

Table 2 illustrates normal estimation results under unoriented angle similarity and PGP metrics. PGP is investigated at three distinct α levels in order to offer a more comprehensive view of our approach's performance. The table draws a comparison between our proposed pipeline trained with different types of neighborhoods and optimizing either dimensionality or eigenvalues entropy objective functions and the baseline. Moreover, it provides results over training points gathered with a sample percentage as discussed

Table 1: Entropy results on training/testing points between classical baseline vs. adaptable neighborhoods, estimated using our pipeline for both spherical and K nearest neighborhoods. The lower values indicate better performance.

Neighborhood Type	Eigen Entropy (train / test)	Dimensionality Entropy (train / test)
Classic	0.8279 / 0.8279	0.8443 / 0.8436
Spherical Neighborhood	0.7365 / 0.7231	0.645 / 0.6456
K nearest neighbors	0.7185 / 0.7127	0.6431 / 0.6295

Table 2: Normal estimation results on training points between classical baseline vs. adaptable neighborhoods estimated using our pipeline for both spherical and K nearest neighborhoods. The higher values indicate better performance.

Neighborhood Type	Objective Function	Angular Similarity	PGP 5	PGP 10	PGP 30
Classic	N/A	0.6769	0.2029	0.3380	0.6140
Spherical Neighborhood	Dimension Entropy	0.6849	0.2542	0.3839	0.6211
	Eigen Entropy	0.6953	0.2771	0.4093	0.6421
K nearest neighbors	Dimension Entropy	0.6856	0.2563	0.3865	0.6213
	Eigen Entropy	0.6856	0.2563	0.3865	0.6213

Table 3: Normal estimation results on test points between classical baseline vs. adaptable neighborhoods estimated using our pipeline for both spherical and K nearest neighborhoods. The higher values indicate better performance.

Neighborhood Type	Objective Function	Angular Similarity	PGP 5	PGP 10	PGP 30
Classic	N/A	0.6778	0.2038	0.3384	0.6169
Spherical Neighborhood	Dimension Entropy	0.6880	0.2550	0.3849	0.6258
	Eigen Entropy	0.6981	0.2804	0.4127	0.6463
K nearest neighbors	Dimension Entropy	0.6773	0.2070	0.3424	0.6167
	Eigen Entropy	0.6773	0.2070	0.3424	0.6167

earlier. The results reveal that optimal neighborhood selection has a positive influence on the normal estimation results. The proposed pipeline outperforms the classical approach by a significant margin, with the spherical neighborhood trained by eigen entropy as the objective function being the best-performing setting. When compared to the baseline, this setting provides a 2% improvement in unoriented angular similarity and a 4% improvement in PGP on average.

The results are extended in Table 3 to include unseen test points. The results confirm that the spherical neighborhood has the highest capacity to generalize across unseen data. Hence, we can conclude based on both Tables 2, 3 that the best fitting choice for normal estimation is a symmetric (spherical) neighborhood with an equivalent dispersion in all directions selected to minimize eigen entropy.

5 FUTURE WORK

For future work, it should be investigated whether the learned neighborhood estimation can generalize not only on points in the same PCD but also on points from different PCDs that have similar structure or belong to the same class. The proposed approach may additionally be validated on other datasets similar to ModelNet such as PCPNet (Guerrero et al., 2018) and is planned to be addressed in future works. Additionally, the pipeline should be extended and validated on large-scale PCDs with millions of points. Our hypothesis is that employing our pipeline will have a positive effect, as empirical results provided in LPDNet (Liu et al., 2019) have shown that an optimal neighborhood selection has a positive effect on the network performance, yet the grid search used in this work has a large memory and computation overhead. Different sampling techniques should be investigated on a large scale PCDs. One good candidate is using spatial clustering over a PCD to create coarse regions of interest, followed by FPS over the clustered areas. The initial clustering stage has the advantage of providing an approximate count of the number of objects in the scene, which helps FPS to sample points that summarize the structure of the different objects. Finally, the design of neighborhood selection heuristics and objective functions is still a work in progress, which can be tailored to reduce errors in neighborhood attributes like the normal vector.

6 CONCLUSION

In this work, we proposed a novel and efficient pipeline for neighborhood estimation given PCDs, which is a major challenge for both machine learning and deep learning methods. The proposed pipeline uses a modification of Deep Neuro-Evolution as a learning module and FPS for intelligent sampling. Besides, a novel fitness function is proposed to evaluate the quality of each individual to reveal the elite solution by applying random mutations of the network parameters for a pre-determined number of generations. To further improve pipeline efficiency, we propose to use only 5% of sampled points and utilize them for the learning phase, while the remaining 95% of points' neighborhood is used to estimate the pipeline generalization performance. In comparison to the baseline, the pipeline was able to reduce entropy values regardless of the neighborhood type. Furthermore, the pipeline has a positive impact on the normal estimation problem, with spherical neighborhoods that optimize eigenvalues entropy delivering the best results.

REFERENCES

Bello, S. A., Yu, S., Wang, C., Adam, J. M., and Li, J. (2020). Deep learning on 3d point clouds. *Remote Sensing*, 12(11):1729.

Ben-Shabat, Y. and Gould, S. (2020). Deepfit: 3d surface fitting via neural network weighted least squares. In *European conference on computer vision*, pages 20–34. Springer.

Ben-Shabat, Y., Lindenbaum, M., and Fischer, A. (2019). Nesti-net: Normal estimation for unstructured 3d point clouds using convolutional neural networks. In *Proceedings of the IEEE/CVF Conference on Computer Vision and Pattern Recognition*, pages 10112–10120.

Chai, J., Zeng, H., Li, A., and Ngai, E. W. (2021). Deep learning in computer vision: A critical review of emerging techniques and application scenarios. *Machine Learning with Applications*, 6:100134.

Cirujeda, P., Mateo, X., Dicente, Y., and Binefa, X. (2014). Mcov: a covariance descriptor for fusion of texture and shape features in 3d point clouds. In *2014 2nd International Conference on 3D Vision*, volume 1, pages 551–558. IEEE.

Demantké, J., Mallet, C., David, N., and Vallet, B. (2011). Dimensionality based scale selection in 3d lidar point clouds. In *Laserscanning*.

Eldar, Y., Lindenbaum, M., Porat, M., and Zeevi, Y. Y. (1994). The farthest point strategy for progressive image sampling. *Proceedings of the 12th IAPR International Conference on Pattern Recognition, Vol. 2 - Conference B: Computer Vision & Image Processing. (Cat. No.94CH3440-5)*, pages 93–97 vol.3.

Fiolka, T., Stückler, J., Klein, D. A., Schulz, D., and Behnke, S. (2012). Sure: Surface entropy for distinctive 3d features. In *International Conference on Spatial Cognition*, pages 74–93. Springer.

Flint, A., Dick, A., and Van Den Hengel, A. (2007). Thrift: Local 3d structure recognition. In *9th Biennial Conference of the Australian Pattern Recognition Society on Digital Image Computing Techniques and Applications (DICTA 2007)*, pages 182–188. IEEE.

Glorot, X. and Bengio, Y. (2010). Understanding the difficulty of training deep feedforward neural networks. In *Proceedings of the thirteenth international conference on artificial intelligence and statistics*, pages 249–256. JMLR Workshop and Conference Proceedings.

Guerrero, P., Kleiman, Y., Ovsjanikov, M., and Mitra, N. J. (2018). Pcpnet learning local shape properties from raw point clouds. In *Computer Graphics Forum*, volume 37, pages 75–85. Wiley Online Library.

Huang, J. and You, S. (2012). Point cloud matching based on 3d self-similarity. In *2012 IEEE Computer Society Conference on Computer Vision and Pattern Recognition Workshops*, pages 41–48. IEEE.

Johnson, A. and Hebert, M. (1998). Surface matching for object recognition in complex 3-d scenes. to appear in. *Image and Vision Computing*.

Lazaros, N., Sirakoulis, G. C., and Gasteratos, A. (2008). Review of stereo vision algorithms: From software to hardware. *International Journal of Optomechatronics*, 2:435 – 462.

Liu, Z., Zhou, S., Suo, C., Yin, P., Chen, W., Wang, H., Li, H., and Liu, Y.-H. (2019). Lpd-net: 3d point cloud learning for large-scale place recognition and environment analysis. In *Proceedings of the IEEE/CVF International Conference on Computer Vision*, pages 2831–2840.

Marton, Z.-C., Pangercic, D., Blodow, N., Kleinehellefort, J., and Beetz, M. (2010). General 3d modelling of novel objects from a single view. In *2010 ieee/rsj international conference on intelligent robots and systems*, pages 3700–3705. IEEE.

Ming, Y., Meng, X., Fan, C., and Yu, H. (2021). Deep learning for monocular depth estimation: A review. *Neurocomputing*, 438:14–33.

Qi, C. R., Su, H., Mo, K., and Guibas, L. J. (2017a). Pointnet: Deep learning on point sets for 3d classification and segmentation. In *Proceedings of the IEEE conference on computer vision and pattern recognition*, pages 652–660.

Qi, C. R., Yi, L., Su, H., and Guibas, L. J. (2017b). Pointnet++: Deep hierarchical feature learning on point sets in a metric space. *Advances in neural information processing systems*, 30.

Rabbani, T., Van Den Heuvel, F., and Vosselmann, G. (2006). Segmentation of point clouds using smoothness constraint. *International archives of photogrammetry, remote sensing and spatial information sciences*, 36(5):248–253.

Royo, S. and Ballesta-Garcia, M. (2019). An overview of lidar imaging systems for autonomous vehicles. *Applied Sciences*, 9:4093.

Rusu, R. B., Blodow, N., Marton, Z. C., and Beetz, M. (2008a). Aligning point cloud views using persistent feature histograms. In *2008 IEEE/RSJ international* *conference on intelligent robots and systems*, pages 3384–3391. IEEE.

Rusu, R. B., Marton, Z. C., Blodow, N., and Beetz, M. (2008b). Persistent point feature histograms for 3d point clouds. In *Proc 10th Int Conf Intel Autonomous Syst (IAS-10), Baden-Baden, Germany*, pages 119–128.

Salimans, T., Ho, J., Chen, X., Sidor, S., and Sutskever, I. (2017). Evolution strategies as a scalable alternative to reinforcement learning. *arXiv preprint arXiv:1703.03864*.

Siritanawan, P., Prasanjith, M. D., and Wang, D. (2017). 3d feature points detection on sparse and non-uniform pointcloud for slam. In *2017 18th International Conference on Advanced Robotics (ICAR)*, pages 112–117. IEEE.

Such, F. P., Madhavan, V., Conti, E., Lehman, J., Stanley, K. O., and Clune, J. (2017). Deep neuroevolution: Genetic algorithms are a competitive alternative for training deep neural networks for reinforcement learning. *arXiv preprint arXiv:1712.06567*.

Suo, C., Liu, Z., Mo, L., and Liu, Y. (2020). Lpd-ae: latent space representation of large-scale 3d point cloud. *IEEE Access*, 8:108402–108417.

Toshev, A., Mordohai, P., and Taskar, B. (2010). Detecting and parsing architecture at city scale from range data. In *2010 IEEE Computer Society Conference on Computer Vision and Pattern Recognition*, pages 398–405. IEEE.

Triebel, R., Kersting, K., and Burgard, W. (2006). Robust 3d scan point classification using associative markov networks. In *Proceedings 2006 IEEE International Conference on Robotics and Automation, 2006. ICRA 2006.*, pages 2603–2608. IEEE.

Vandapel, N., Huber, D. F., Kapuria, A., and Hebert, M. (2004). Natural terrain classification using 3-d ladar data. In *IEEE International Conference on Robotics and Automation, 2004. Proceedings. ICRA'04. 2004*, volume 5, pages 5117–5122. IEEE.

Varga, D., Szalai-Gindl, J. M., Formanek, B., Vaderna, P., Dobos, L., and Laki, S. (2021). Template matching for 3d objects in large point clouds using dbms. *IEEE Access*, 9:76894–76907.

Wang, Y., Sun, Y., Liu, Z., Sarma, S. E., Bronstein, M. M., and Solomon, J. M. (2019). Dynamic graph cnn for learning on point clouds. *Acm Transactions On Graphics (tog)*, 38(5):1–12.

Wang, Z. and Prisacariu, V. A. (2020). Neighbourhood-insensitive point cloud normal estimation network. *arXiv preprint arXiv:2008.09965*.

Weinmann, M., Jutzi, B., and Mallet, C. (2014). Semantic 3d scene interpretation: A framework combining optimal neighborhood size selection with relevant features. *ISPRS Annals of the Photogrammetry, Remote Sensing and Spatial Information Sciences*, 2(3):181.

Weinmann, M., Schmidt, A., Mallet, C., Hinz, S., Rottensteiner, F., and Jutzi, B. (2015). Contextual classification of point cloud data by exploiting individual 3d neigbourhoods. *ISPRS Annals of the Photogrammetry, Remote Sensing and Spatial Information Sciences II-3 (2015), Nr. W4*, 2(W4):271–278.

Wu, Z., Song, S., Khosla, A., Yu, F., Zhang, L., Tang, X., and Xiao, J. (2015). 3d shapenets: A deep representation for volumetric shapes. In *Proceedings of the IEEE conference on computer vision and pattern recognition*, pages 1912–1920.

Yang, Y., Feng, C., Shen, Y., and Tian, D. (2018). Foldingnet: Point cloud auto-encoder via deep grid deformation. In *Proceedings of the IEEE conference on computer vision and pattern recognition*, pages 206–215.

Zhao, C., Yang, J., Xiong, X., Zhu, A., Cao, Z., and Li, X. (2022). Rotation invariant point cloud analysis: Where local geometry meets global topology. *Pattern Recognition*, 127:108626.

Zhong, Y. (2009). Intrinsic shape signatures: A shape descriptor for 3d object recognition. In *2009 IEEE 12th international conference on computer vision workshops, ICCV Workshops*, pages 689–696. IEEE.

Zhou, J., Jin, W., Wang, M., Liu, X., Li, Z., and Liu, Z. (2021a). Improvement of normal estimation for pointclouds via simplifying surface fitting. *arXiv preprint arXiv:2104.10369*.

Zhou, J., Jin, W., Wang, M., Liu, X., Li, Z., and Liu, Z. (2021b). Improvement of normal estimation for pointclouds via simplifying surface fitting. *ArXiv*, abs/2104.10369.

Zhu, R., Liu, Y., Dong, Z., Wang, Y., Jiang, T., Wang, W., and Yang, B. (2021). Adafit: Rethinking learning-based normal estimation on point clouds. In *Proceedings of the IEEE/CVF International Conference on Computer Vision*, pages 6118–6127.

SCIENCE AND TECHNOLOGY PUBLICATIONS